This paper appears in Mechatronics, vol. 22, no. 1, pp. 1-12, 2012.

Improved Tracking and Switching Performance of an Electro-Pneumatic Positioning System

Sean Hodgson[1], Minh Quyen Le[2], Mahdi Tavakoli[1], Minh Tu Pham[2]

hodgson4@ualberta.ca, minh-quyen.le@insa-lyon.fr, tavakoli@ece.ualberta.ca, minh-tu.pham@insa-lyon.fr

[1]Department of Electrical and Computer Engineering, University of Alberta, Edmonton, AB Canada T6G2V4

[2]Laboratoire Ampère, UMR CNRS 5005, Université de Lyon, INSA-LYON, F-69621 Villeurbanne Cedex, France

Abstract

For robotic systems that use on/off (solenoid) pneumatic actuators, a sliding mode control law for precise position control and low switching (open-close) activity of the valves is presented in this paper. Given a pneumatic actuator with two chambers and four solenoid valves, there are sixteen possible input combinations defined directly from the state of the four on/off valves present in the system; however, only seven of these discrete operating modes are considered both functional and unique. Therefore, we introduce a novel seven-mode sliding controller that minimizes the position tracking error using modes that have both the necessary and sufficient amounts of drive energy and, thus, involve reduced switching activity. An analysis of the closed-loop system stability is carried out. The performance of the proposed control design is experimentally verified on a single pneumatic actuator setup comprising of two chambers with four on/off valves.

Index Terms

Pneumatic actuator, on/off solenoid valve, robot control, sliding mode control, position tracking, switching activity, stability.

I. Introduction

Modern robotic systems have enabled humans to work in environments that are difficult or hazardous to reach or operate in. Robotic systems have been developed for operations ranging from surgery to space exploration. In robot-assisted surgery, for instance, the surgical robot may be required to work in places that have strong magnetic fields such as inside a Magnetic Resonance Imaging (MRI) scanner. An MRI scanner affords pictures with high resolution and contrast, providing surgeons with a patient's three-dimensional visualization [1] in a nearly real-time manner [2]. Robotics-assisted surgery under MRI has the advantage that it can direct the surgical tools to targets not normally visible. Also, the immediate visual feedback during the operation makes the surgery more efficient as the patient does not have to leave the operating room for diagnostic testing.

Despite these benefits, MR images are obtained through the use of strong and precise magnetic fields. No ferromagnetic materials is allowed inside an active MRI. Any ferromagnetic materials in actuators (such as electric motors) or sensors present in the surgical robot will generate noises that make it difficult to scan highly-precise MR images [1]. This represents a severe design limitation for surgical robots that are to work under MRI guidance. As a result, the Intuitive Surgical Inc's da Vinci system – the only clinically-approved and commercially-available surgical robot for soft-tissue surgery – is not MRI compatible [3].

If electric motors are to be used as actuators in MRI-compatible robots, the motors need to be placed far away from the magnetic field and the surgical site [4], creating further design complications. Alternatively, it is possible to use pneumatic actuators to drive the surgical robots; see [5] as an example. This is because pneumatic actuators can be used directly in the magnetic field and are thus completely MRI-compatible [6].

In addition to being inert to magnetic fields, pneumatic actuators offer many advantages for positioning applications such as low maintenance cost, high ratio of power to weight, cleanliness, and safety [7]. However, they suffer from common drawbacks including friction and sensitivity of the actuator dynamics to load and piston position along the cylinder stroke [8]. Also, from a control perspective, controlling a pneumatic actuator is a challenge because the system dynamics are highly nonlinear [9].

To control the input (air) flow in a pneumatic actuator, some pneumatic systems have utilized servovalves [10]. These valves allow for a continuous change of the input mass flow rate. However, servovalves are costly due to the precision machining required in their manufacturing. A low-cost alternative to a servovalve is the on/off solenoid valve, which has as a result found widespread applications. Controllers to compensate for the nonlinearities of servovalve pneumatic systems have been reported [8], [9], [11], [12]. The difficulty is that the nonlinear nature of a pneumatic actuator is worsened when it uses on/off solenoid valves instead of servovalves. In this case, precise control is difficult due to the discrete-input nature of the system.

Past research has developed solenoid-valve pneumatic systems, which utilize a pulse width modulated (PWM) controller [13], [14], [15], [16]. Using time averaging, a PWM input with a sufficiently high frequency can approximate the continuous input properties of a servovalve [11]. While the nonlinear dynamics of a solenoid-valve pneumatic system can be approximated as an equivalent linear system [7], the highly nonlinear nature of such a system precludes the use of linear controllers. It is possible to use nonlinear model averaging techniques combined with PWM and sliding control [11] or direct sliding mode control for solenoid-valve systems [17]. Sliding mode control is a form of variable structure nonlinear control that alters the dynamics of the system by the application of a high-frequency switching control [18], [19]. Sliding mode control can account for the nonlinearities of the system as well as its dynamic uncertainties [17].

A. Sliding Control of Solenoid-Valve Actuators

In this paper, we consider a pneumatic actuator comprised of two chambers as shown in Figure 1. Each chamber has two solenoid valves, each of which can be either closed, connected to a compressed air supply (source pressure), or to exhaust (atmosphere pressure). With four solenoid valves, one would assume that there would be a total of sixteen discrete modes for the actuator at any given time. However, since we cannot have a chamber connected to pressure and exhaust at the same time, only nine discrete modes exist. If we assume the three modes in which both chambers are closed, both chambers are venting, and both chambers are pressurizing are functionally equivalent (which is true under the no load case) then the system has a total of seven unique discrete modes.

A sliding mode controller can force the open-loop system to transition between these discrete operating modes, which were defined directly from the state of the on/off solenoid valves, with the transition between the modes decided based on the current tracking error. In [17], three discrete modes are considered for a two-chamber solenoid-valve actuator (same as Figure 1):

- Push and Pull (chamber P connected to supply pressure and chamber N connected to exhaust pressure)

- Pull and Push (chamber P connected to exhaust pressure and chamber N connected to supply pressure)
- Closed and Closed (both chambers' valves closed)

One of the contributions of this paper is to expand the three-mode open-loop model of [17] into a seven-mode open-loop model. The new system has four extra modes, which facilitate the use of more optimal amounts of drive energy for good positioning precision and reduced valve switching (open-close) activity. These four additional modes considered for the two-chamber actuator are:

- Push and Close (chamber P connected to supply pressure and chamber N is closed)
- Pull and Close (chamber P connected to exhaust pressure and chamber N is closed)
- Close and Push (chamber N connected to supply pressure and chamber P is closed)
- Close and Pull (chamber N connected to exhaust pressure and chamber P is closed)

Due to one chamber being closed, each of the above 4 modes involves a reduced amount of drive energy (and piston acceleration) as compared to the original 3-modes. This can allow for the delivery of optimal amounts of drive energy to the actuator, thus enabling more subtle adjustments to the piston position. By making fine position adjustments and thus avoiding piston overshoot, fewer valve switches will be required. The result is improved positioning accuracy and reduced switching activity for the controlled system.

Another contribution of this paper compared to the 3-mode design is in providing guidelines for the selection of threshold values used by the sliding controller to decide switching between the discrete operating modes of the open-loop system. The controller will use these thresholds for transition from one mode to another mode based on the full state of the system: piston position, velocity, and acceleration as well as chamber pressures. By optimizing these transition thresholds, we can decrease the switching activity of the on/off solenoid valves, which increases their operating lifespan.

The organization of this paper is as follows: The modeling of the pneumatic actuator with its chamber and four solenoid valves is reported in Section II. The discrete input model of the actuator is given in Section III. The operation and design of the sliding controller are discussed in Section IV. The simulation study to verify the control laws is in Section V. The experimental results are presented in Section VI while Section VII contains the concluding remarks.

II. Open-Loop Pneumatic Actuator Model

This section of the paper derives the open-loop model of the pneumatic actuator including its on/off solenoid valves as shown in Figure 1. To describe the air flow dynamics in a cylinder, we assume that:

- Air is a perfect gas and its kinetic energy is negligible in the chamber,
- The pressure and the temperature are homogeneous in each chamber,
- The evolution of the gas in each chamber is polytropic.
- The temperature variation in chambers is negligible with respect to the supply temperature,
- The mass flow rate leakages are negligible, and
- The supply and exhaust pressures are constant.

The Simscape simulations in Section V do not assume/model all of these assumptions.

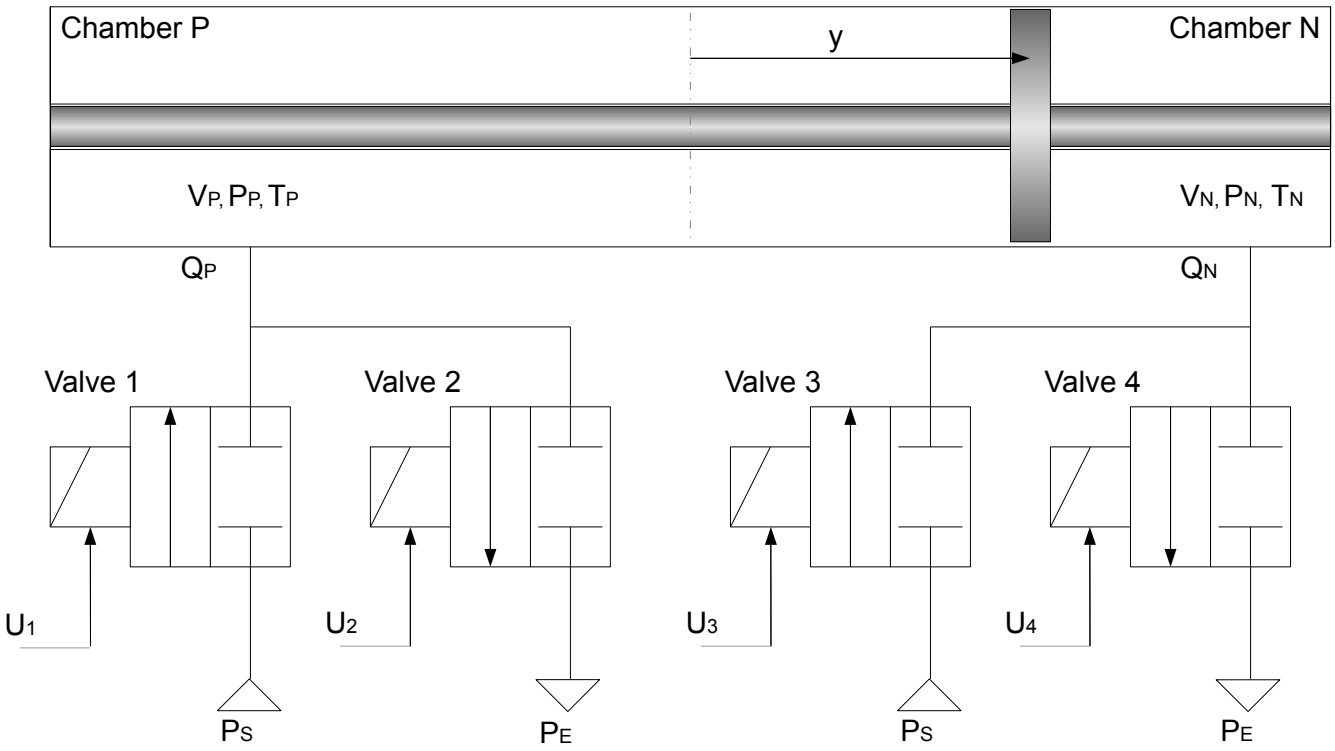

Fig. 1. Electro-pneumatic system with 4 on/off solenoid valves.

A. Pneumatic Chambers

If the charging and discharging of the chambers' cylinders are assumed to be polytropic, then the pressure dynamics of these chambers can be approximated [20] as

$$\dot{P}_P = \frac{k}{V_P}(rTQ_P - AP_P\dot{y}) \qquad \dot{P}_N = \frac{k}{V_N}(rTQ_N + AP_N\dot{y}) \tag{1}$$

where P_P and P_N refer to pressures (Pa) inside the chambers P and N, respectively, Q_P and Q_N refer to mass flow rates (kg/s) of the chambers P and N, respectively, A_P and A_N refers to the piston cylinder area's (m^2) inside the chambers P and N, respectively, T refers to the chamber temperature (K), k refers to the polytropic constant, r refers to the universal gas constant (J/(kgK)), and y refers to the piston position (m) shown in Figure 1. Note the arrows for position y, Force (N) F_{Ext} and F_{st} shown in Figure 1 refer to their positive directions, a negative magnitude to any of these quantities will refer to the opposite direction. V_P and V_N refer to volumes (m^3) of the chambers P and N, respectively as shown below:

$$V_P = A(l/2 + y) \quad V_N = A(l/2 - y) \tag{2}$$

B. Valves

The mass flow rates Q_P and Q_N can be derived in terms of the discrete voltage inputs U_1, U_2, U_3 and U_4 shown in Figure 1 and the continuous pressure inputs P_P and P_N. Please note $U_i \in \{0, 1\}$.

$$Q_P = U_1 Q(P_S, P_P) - U_2 Q(P_P, P_E) \tag{3a}$$

$$Q_N = U_3 Q(P_S, P_N) - U_4 Q(P_N, P_E) \tag{3b}$$

Here, P_S and P_E are the pressures of the supply and the exhaust.

In general, Q(P_{Up},P_{Down}) used in (3a) and (3b), in which P_{Up} is the upstream pressure and P_{Down} is the downstream pressure, refers to the expression for the mass flow rate through an orifice. This generalized model has two parameters to describe the mass flow rate: the critical pressure ratio $b = 0.433$ and the mass flow rate constant $C_{val} = C\rho_0$ [21]. Where C is the sonic conductance and ρ_0 is the density of air at reference condition (T_0 = 293 K).

$$Q(P_{Up}, P_{Down}) = C_{val} P_{Up} \sqrt{\frac{T_{Atm}}{T_{Up}}} \times \begin{cases} \sqrt{1 - \left(\frac{\frac{P_{Down}}{P_{Up}} - b}{1-b} \right)^2} & \text{, if } \frac{P_{Down}}{P_{Up}} > b \text{ (subsonic)} \\ 1 & \text{, if } \frac{P_{Down}}{P_{Up}} \leq b \text{ (choked)} \end{cases} \tag{4}$$

The value for b comes directly from the datasheet of the solenoid valves, provided by Matrix-Bibus (BIBUS France S.A.S, Chaponnay, France). In the above, T_{Up} is the upstream temperature of air and T_{Atm} is the atmospheric temperature. Also, C_{Val} is a characteristic of the valve.

C. Piston

Finally, the dynamics of the mechanical actuator involving the applied force on the piston and the resulting piston motion is

$$A(P_P - P_N) - b_m \dot{y} + F_{Ext} - F_{St} = M_m \ddot{y} \tag{5}$$

where b_m is the viscose coefficient (N s/m), M_m is the total mass of the load and the piston (Kg), F_{St} is the stiction force (N), and F_{Ext} is the external force (N). F_{St} was considered to be negligible since the pneumatic actuator used in experiment was an Airpel anti-stiction cylinder (ALL AIR Inc, New York, US).

III. Modelling of the Open-Loop Actuator as a Discrete-Input System

It is possible to combine the equations in Section II to write the dynamics of the open-loop pneumatic actuator in a 7-mode discrete-input. Differentiating (5) solving for $\dddot{y}$ and substituting (1) and (2) in it, the dynamics of the actuator are obtained as

$$\dddot{y} = \frac{-b_m}{M_m} \ddot{y} - \frac{Ak}{M_m} \left(\frac{P_P}{l/2 + y} + \frac{P_N}{l/2 - y} \right) \dot{y} + \frac{krT}{M_m} \left(\frac{Q_P}{l/2 + y} - \frac{Q_N}{l/2 - y} \right)$$

where l is the total length of the chamber.

As mentioned before, only one of the two valves U_3 and U_4 can be open at any given time to avoid a bypass of the chamber N. Similarly, only one of the two valves U_1 and U_2 can be open at any given time to avoid a bypass of the chamber P. From this, we find that there are a total of nine discrete modes for the solenoid valves [20]. These modes are shown in Table I.

Reviewing these different discrete modes, we observe that modes M_1, M_8 and M_9 are functionally similar (under no load) as they correspond to the two chambers being both closed, both venting, and both pressurized, respectively. For all of these three modes, the pressure difference across the chamber P and chamber N is reduced to zero over time. In fact according to (5), the acceleration of the piston is influenced by the *difference* in pressures of the two chambers and, thus, from a functional perspective under no load these three modes are the same.

To reduce functional and tuning complexity as well as to reduce system switching this paper will outline a controller that only utilizes seven modes. These modes are M_1 through M_7 of the open-loop system. M_1 was selected out of the three (M_1, M_8 and M_9) because it has the highest resistance to piston motion which will improve system performance while under load.

TABLE I
NINE DISCRETE MODES OF THE OPEN-LOOP ACTUATOR.

	M_1	M_2	M_3	M_4	M_5	M_6	M_7	M_8	M_9
U_1	0	1	0	0	0	1	0	0	1
U_2	0	0	1	0	0	0	1	1	0
U_3	0	0	0	0	1	0	1	0	1
U_4	0	0	0	1	0	1	0	1	0

From a functional perspective, we can describe the seven different operating modes listed in Table I. In the operating mode M_1, both chambers are closed, as a result it has no active influence (i.e., actuation) on the system. In the operating mode M_2, chamber N is closed and chamber P is pressurized, thus the piston moves to the right. In the operating mode M_3, chamber N is closed and chamber P is exhausted (connected to atmosphere), thus the piston moves to the left. In the operating mode M_4, chamber P is closed and chamber N is exhausted, again moving the piston to the right. In the operating mode M_5, chamber P is closed and chamber N is pressurized, again moving the piston to the left.

In the operating modes M_2 to M_5 one chamber is closed while the other is pressurized or exhausted, which makes the piston motion limited because one chamber is closed. In the operating mode M_6, however chamber P is pressurized and chamber N is exhausted, moving the piston *as forcefully as possible* to the right. In the operating mode M_7, chamber P is exhausted and chamber N is pressurized, moving the piston *as forcefully as possible* to the left.

For the seven discrete modes, dynamic equation can be obtained by substituting (3a) and (3b) into (6). We obtain

$$\dddot{y} = \begin{cases} F(Z) & \text{, mode } M_1 \\ F(Z) + (-1)^i B_i(Z) & \text{, mode } M_i,\ (2 \leq i \leq 7) \end{cases} \tag{6}$$

where $Z = \{y, \dot{y}, \ddot{y}, P_P, P_N\}$ is the state vector and

$$B_2(Z) = \frac{krT}{M_m}\frac{Q(P_S, P_P)}{(l/2+y)} \qquad B_3(Z) = \frac{krT}{M_m}\frac{Q(P_P, P_E)}{(l/2+y)}$$
$$B_4(Z) = \frac{krT}{M_m}\frac{Q(P_N, P_E)}{(l/2-y)} \qquad B_5(Z) = \frac{krT}{M_m}\frac{Q(P_S, P_N)}{(l/2-y)}$$
$$B_6(Z) = B_2(Z) + B_4(Z) \qquad B_7(Z) = B_5(Z) + B_3(Z)$$

$$F(Z) = \frac{-b_m}{M_m}\ddot{y} - \frac{Ak}{M_m}\left(\frac{P_P}{l/2+y} + \frac{P_N}{l/2-y}\right)\dot{y}$$

Note that because $P_E \leq P_P \leq P_S$, $P_E \leq P_N \leq P_S$ and $-l/2 \leq y \leq l/2$ and mass flow rates are non-negative functions $B_2(Z)$ through $B_7(Z)$ are all positive or equal to zero.

IV. Sliding Mode Controller Design

The proposed controller reacts differently depending on which of the seven modes the open-loop system is in at any given time. For a position-controlled system, we can define as the following sliding surface $s = 0$ where s is defined as:

$$s = \frac{\ddot{e}}{\omega^2} + \frac{2\xi\dot{e}}{\omega} + e \tag{7}$$

where e is the position error $y - y_d$, y is the actual position, y_d is the desired position, and ξ and ω are constant and positive numbers.

TABLE II
Selection of the operating mode based on positioning error s.

Region	Discrete operating modes	Magnitude of $\dot{s}$ from (12)
$s > \beta$	M_7	Large negative
$\beta \geq s > \epsilon$	M_3 and M_5	Modest negative
$\epsilon \geq s > -\epsilon$	M_1	Minimal
$-\epsilon \geq s > -\beta$	M_2 and M_4	Modest positive
$-\beta \geq s$	M_6	Large positive

We use this the function s from (7) and invoke the seven different modes of the open-loop system based on five different regions of the s function. These regions of s and the selected operating mode of the system are illustrated in Table II – we will see the meaning of the last column in the next subsection. Please note that the input voltages (i.e., control actions) for each mode are listed in Table I. If we employ a pneumatic controller based on Table II, for the lowest error $|s| < \epsilon$, we use the mode M_1 which has no active influence on the system. For the largest positive error $s > \beta$, we use the mode M_7, which exerts the highest active influence in the negative direction on the system. Conversely, for the largest negative error $s < -\beta$, we use the mode M_6, which has the highest active influence in the positive direction.

In the next three subsections, first we discuss how closed-loop stability is guaranteed if the sliding controller properly transitions the open-loop system between its discrete operating modes. Next, within the stabilizing sliding control framework,

we establish a hierarchy for transition between admissible modes such that closed-loop performance is improved. Then, we provide guidelines on the choice of threshold values that decide the transitions between modes.

A. Stability

To be able to analyze stability, consider the Lyapunov function candidate

$$V_{lya} = \frac{1}{2}s^2 \tag{8}$$

V_{lya} is a positive-valued function, therefore, if $\dot{V}_{lya} < 0$, V_{lya} will be decreasing. If V_{lya} is decreasing, $|s|$ will also be decreasing. Assuming s is initially bounded and $|s|$ is always decreasing, then s will always be bounded. Here, s will asymptotically approach zero if we control the system so that

$$\dot{V}_{lya} = \dot{s}s < -\eta|s| \tag{9}$$

for some constant $\eta > 0$ [18][19][17]. This condition can be rewritten as

$$\begin{cases} \dot{s} > \eta & if s < 0 \\ \dot{s} < -\eta & if s > 0 \end{cases} \tag{10}$$

Take the derivative of (7) to get

$$\dot{s} = \frac{\ddot{e}}{\omega^2} + \frac{2\xi\ddot{e}}{\omega} + \dot{e} = \frac{\dddot{y} - \dddot{y}_d}{\omega^2} + \frac{2\xi\ddot{e}}{\omega} + \dot{e} \tag{11}$$

By substituting (6) into (11) we obtain

$$\dot{s} = \begin{cases} \lambda & , mode\ M_1 \\ \lambda + (-1)^i B_i(Z)/\omega^2 & , mode\ M_i,\ (2 \leq i \leq 7) \end{cases} \tag{12}$$

where $\lambda = (F(Z) - \dddot{y}_d)/\omega^2 + 2\xi\ddot{e}/\omega + \dot{e}$.

λ will be bounded if $\dot{y}$, $\ddot{y}$, $\dot{y}_d$, $\ddot{y}_d$, $\dddot{y}_d$, P_P, and P_N are bounded. P_P and P_N are bounded between P_S and P_E. y_d is a controlled input to the system thus y_d, $\dot{y}_d$, $\ddot{y}_d$, $\dddot{y}_d$ are assumed to be bounded. If we rewrite the (5) as

$$M_m\ddot{y} + b_m\dot{y} = A(P_P - P_N) \tag{13}$$

we see that the right side of (13) is always bounded. Therefore, (13) is a 1^{st} order differential equation in terms of the velocity ($\dot{y}$), which means velocity is decaying exponentially if M_m and b_m are positive. Therefore, if $\dot{y}$ is initially bounded, then $\dot{y}$ will always be bounded. If we rewrite (5)

$$\ddot{y} = \frac{1}{M_m}(A(P_P - P_N) - b_m\dot{y}) \tag{14}$$

We find that it is defined purely in terms of bounded functions, thus it too must always be bounded. Therefore, λ is also bounded.

Therefore, if the positive-valued functions $B_2(Z)$, $B_4(Z)$, $B_6(Z)$ are sufficiently large, then modes M_2, M_4 and M_6 can ensure $\dot{s} > \eta$; this is appropriate when s is negative. Conversely, if the positive-valued functions $B_3(Z)$, $B_5(Z)$ and $B_7(Z)$ are sufficiently large, then modes M_3, M_5 and M_7 can ensure $\dot{s} < -\eta$; this is appropriate when s is positive. These two facts will be used to design a control strategy that satisfies (9).

All six functions $B_2(Z)$ to $B_7(Z)$ are linearly proportional to C_{val}, the valve's mass flow rate constant in (4), thus choosing a large enough valve will ensure that these scalar functions will be sufficiently large. Thus, using the modes M_2, M_4 and M_6 when $s < 0$, and using M_3, M_5 and M_7 when $s > 0$ will ensure (9), and thus the convergence to the sliding surface $s = 0$ over time.

If s converges to zero and y_d, $\dot{y}_d$, $\ddot{y}_d$ are bounded the output y, $\dot{y}$, $\ddot{y}$ will also be bounded and thus the system will be BIBO stable.

B. Mode Selection

The 7-mode controller requires knowledge of the current chamber pressures as well as the current piston position to pick the appropriate operating modes. This requires additional sensors as compared to the 3-mode controller. For the case where we are trying to regulate to a stationary y_d, we can use this additional mode data to minimize the switching required to bring y to y_d.

While there are unique control choices when $|s| > \beta$ or $|s| < \epsilon$, we require conditions for deciding which control mode to use when $\beta \geq |s| > \epsilon$ (see Table II). For the positive region and the negative region there are two control modes: (M_5 and M_3) and (M_2 and M_4), respectively.

We will first study the negative region $-\beta \geq s > -\epsilon$. For the operating mode M_2, the chamber P is pressurized and chamber N is closed causing a moderate positive acceleration. If we evaluate (5) under mode M_2 and assume that the filling chamber has a sufficient amount of time to be fully pressurized we can see that the $\ddot{y} \propto (P_S - P_N)$. For operating mode M_4, the chamber N is being exhausted and chamber P is closed, also causing a moderate positive acceleration. If we evaluate (5) under mode M_4 and assume that the venting chamber has a sufficient amount of time to be fully vented we can see that the $\ddot{y} \propto (P_P - P_E)$

If we define

$$E_1 \quad = \quad (P_S - P_N) - (P_P - P_E) = (P_S + P_E) - (P_P + P_N) \tag{15}$$

the magnitude of E_1 is positive when the pressure difference $P_S - P_N$ is greater than the pressure difference $P_P - P_E$. Therefore, when E_1 is positive, the appropriate operating mode for the region $-\epsilon \geq s > -\beta$ is M_2 as it will result in a higher

piston acceleration compared to the mode M_4. Conversely when the magnitude of E_1 is negative M_4 will result in a higher piston acceleration compared to M_2.

In the positive region $\beta \geq s > \epsilon$, comparing modes M_5 and M_3, from (5) we see that the magnitudes of $\ddot{y}$ are based on the pressure differences $P_S - P_P$ and $P_N - P_E$ respectively. Let us define

$$E_2 \quad = \quad (P_S - P_P) - (P_N - P_E) = (P_S + P_E) - (P_P + P_N) = E_1 \tag{16}$$

The magnitude of E_2 is positive when the pressure difference $P_S - P_P$ is greater then the pressure difference $P_N - P_E$. Therefore, when E_2 is positive the appropriate operating mode for the region $\epsilon \geq s > \beta$ is M_5 as it will accelerate the piston more compared to mode M_3. Conversely when the magnitude of E_2 is negative mode M_3 will result in a higher piston acceleration compared to M_5

In summary, the magnitude of s in (7) and the magnitude of E_1 in (15) can be used by the controller to select the best of the seven operating modes see Figure 2.

C. Selecting Parameters τ, β and ϵ

This section proposes appropriate ways for selecting the controller parameters of τ, β and ϵ for smoothest motions and least switching activity. For these parameters, the criterion for threshold selection was not unique. We chose the β and τ parameters based primarily on the velocity error. Refer to Table IV for a summary of tuning parameters.

1) Selecting τ: The purpose of the timeout parameter τ is to reduce switching between the modes used in the region $\beta \geq |s| > \epsilon$ by enforcing a minimum amount of time between mode transitions: M_5 to M_3, M_3 to M_5, M_2 to M_4 and M_4 to M_2. A larger τ value will reduce switching , by limiting transitions. If the τ value is reduced switching will increase, but the velocity output of the system will be a more consistent output resulting in improved tracking performance. This is a performance trade-off, therefore, an appropriate value of τ should be determined by evaluating the open-loop responses M_2 and M_4.

For initial conditions (at $t = 0$) of $y = 0$ and $V_P = V_N = A\frac{l}{2}$ (i.e., the piston positioned in halfway along the cylinder length), using (1) - (5) we can simulate the open-loop system response in each of these modes (Figure 3). These initial conditions were selected because they are symmetric in nature, as such the modes M_5 and M_3 will be symmetric to modes M_2 and M_4.

For the pressurizing case M_2 the initial conditions $P_P = P_N = P_E$ were selected. For the venting case M_4 the initial conditions $P_P = P_N = P_S$ were selected.

Evaluating the consistency of the output velocity of these two modes in Figure 3(a), we see there is not a large variation in terms of the output velocity between 20 ms and 40 ms. As the switching activity is inversely related to the timeout value, we select the higher value of $\tau = 40$ ms to minimize switching. Thus, a minor change in the timeout τ will have a minimal impact in terms of tracking performance.

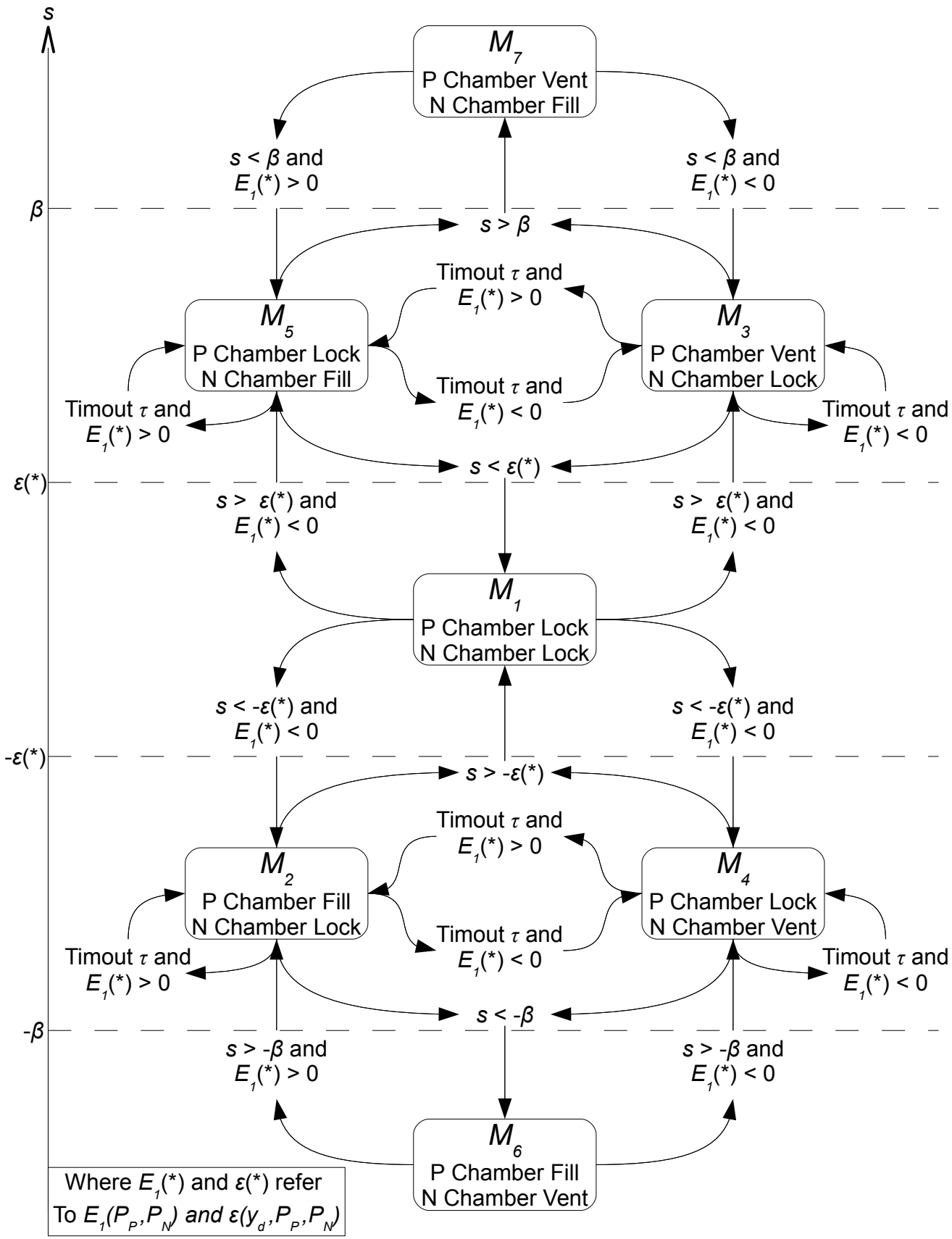

Fig. 2. 7-mode controller diagram.

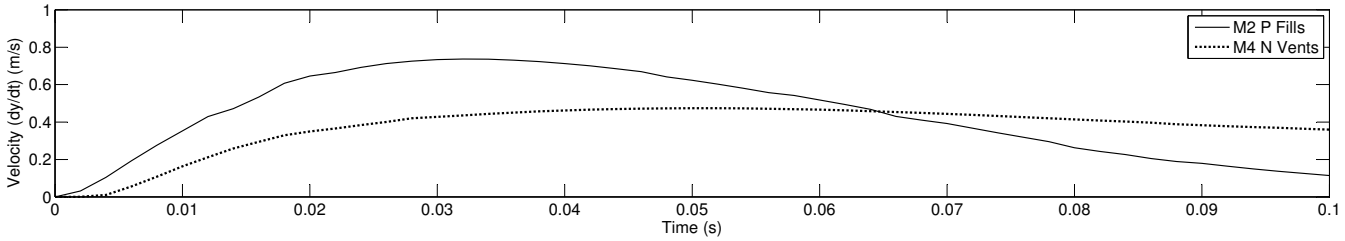

(a) Piston Velocity (m/s)

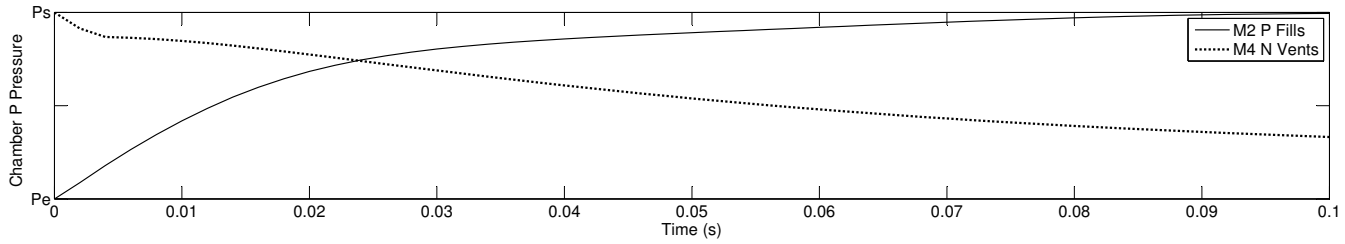

(b) Chamber P Pressure

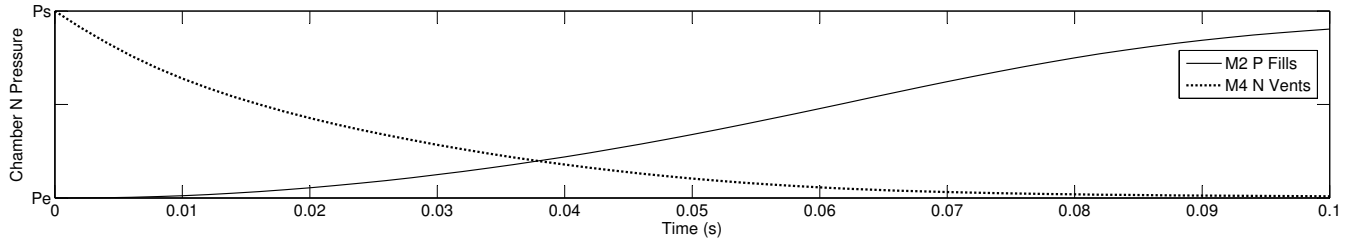

(c) Chamber N Pressure

Fig. 3. Open-loop responses modes M_2 and M_4.

2) Selecting β: The magnitude β is the transition threshold between a mode connecting the two chambers to supply and exhaust pressures (i.e., M_6 or M_7), and the alternating modes for opening only a single valve (i.e., M_2/M_4 or M_3/M_5). To improve our understanding of this, we will evaluate the steady states of two different operating regions (from Table II) : the region $s \leq -\beta$ (i.e., mode M_6) and the region $-\epsilon \geq s > -\beta$ (i.e., modes M_2 and M_4 alternating). Observe the open-loop responses of M_6 and M_2/M_4 in Figure 4. These open-loop responses were generated using the same initial conditions as seen in the previous sections pressurizing case . As it can be seen from Figure 4 the velocity of the piston increases to a maximum. If we approximate the nominal velocity in each region to be half of its maximum velocity, we can select the mode transition threshold between the two regions as the average of the region's nominal velocities.

To approximate the maximum piston velocity we select the following conditions to maximize the velocity: $\ddot{y} = 0$, $F_{St} = 0$, $P_P = P_S$, $P_N = P_E$, and $F_{Ext} = 0$. Substituting these conditions into (5) we find the maximal velocity as

$$max(\dot{y}) = \frac{A(P_S - P_E)}{b_m} \tag{17}$$

From a time averaged perspective, the M_2/M_4 modes have approximately half the air flow (of the M_6 mode) since only half the orifices are open at any given time. Thus the M_2/M_4 modes maximum velocity can be approximated as half of $max(\dot{y})$. From this, the nominal velocity of each region can be approximated as $\frac{1}{2}max(\dot{y})$ and $\frac{1}{4}max(\dot{y})$, making the transition threshold

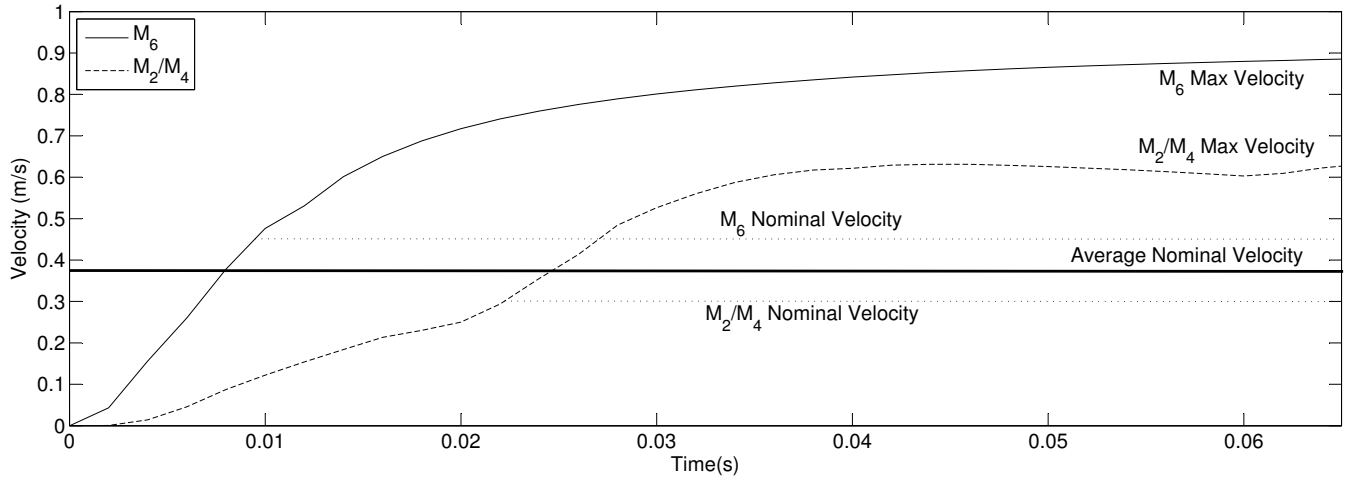

Fig. 4. Open-loop responses of modes M_6 and M_2/M_4.

equal to $\frac{1}{2}(\frac{1}{2}max(\dot{y}) + \frac{1}{4}max(\dot{y})) = \frac{3}{8}max(\dot{y})$. In terms of β we multiply the threshold by $\frac{2\xi}{\omega}$ to convert this transition point into the function s in (7) to get:

$$\beta = \frac{3\xi}{4\omega}max(\dot{y}) = \frac{3\xi A(P_S - P_E)}{4b_m\omega} \tag{18}$$

This selection of β is not unique however it has been demonstrated in simulation results as being appropriate.

3) Selecting ϵ: When the magnitude of s is less than a positive valued but small ϵ, the controller removes the actuation from the system by closing all valves. The magnitude of ϵ should ideally be selected so that when this occurs and the effect of past actuations settles out, the position difference, $y - y_d$, will be less than some desired small amount e_{min}. Here, e_{min} is an appropriate value for ϵ for tracking a non-stationary desired position ($\dot{y_d} \neq 0$). However, when the system is moving towards a stationary desired position ($\dot{y_d} = 0$) and the valves of the system are closed (for both chambers P and N), the piston does not immediately stop. The pressure difference between chambers P and N when the valves are shut will go to zero only after the final position has overshot past the desired position. Ideally, the system should have shut all the valves before reaching the desired position so that the final settled position y would be close to y_d.

When the valves are shut, all flow rates are equal to zero (i.e., $Q_P = Q_N = 0$). For initial pressures P_N and P_P and final pressures P_{PF} and P_{NF}, the total molecules in each chamber will be the same. Thus, the initial pressure and final pressure can be equated as follows

TABLE III
ϵ TRANSITION TABLE.

	Intial state	Final state
Pressure	$P_P \neq P_N$	P_{PF}, P_{NF}
Position	y	y_f
Velocity	$\dot{y} \neq 0$	$\dot{y}_f = 0$
Acceleration	$\ddot{y} \neq 0$	$\ddot{y}_f = 0$

$$PV = P_F V_F \tag{19}$$

based on the ideal gas law (refer to Table III). From this, we find the following relationships between pressures and positions

$$P_{PF}A(\frac{l}{2}+y_f) = P_PA(\frac{l}{2}+y) \quad P_{NF}A(\frac{l}{2}-y_f) = P_NA(\frac{l}{2}-y) \tag{20}$$

where y is the initial position and y_f is the final position. This equation assumes a k value of 1 to simplify the math. Therefore, the selection of the ϵ threshold is based on this simplification.

By evaluating (5) at the stationary point ($\ddot{y} = \dot{y} = 0$) and substituting (20), we obtain

$$\begin{gathered}(P_{PF} - P_{NF}) = 0 \\ P_P\frac{\frac{l}{2}+y}{\frac{l}{2}+y_f} - P_N\frac{\frac{l}{2}-y}{\frac{l}{2}-y_f} = 0\end{gathered} \tag{21}$$

Solving for y and substituting y_d for the final position y_f, we find

$$y = \frac{P_N(y_d+\frac{l}{2})l}{P_N(y_d+\frac{l}{2}) + P_P(\frac{l}{2}-y_d)} - \frac{l}{2} \tag{22}$$

Solving for e we find

$$e = \frac{P_N y'_d l}{P_N y'_d + P_P(l-y'_d)} - y'_d \tag{23}$$

where $y'_d = y_d + \frac{l}{2}$.

Immediately after the system switches to mode M_1, the pistons position y is approaching y_d and, therefore, e will be either a positive or negative value with a sign opposite the sign of $\dot{y}$. Since the threshold ϵ is always a positive magnitude, we are interested in $|e|$. We convert this transition point into the function s in (7) to get:

$$s_{stop} = \left| \frac{P_N y'_d l}{P_N y'_d + P_P(l-y'_d)} - y'_d) \right| \tag{24}$$

To utilize this threshold in experiment two conditions must be met: The equation (24) requires $\dot{y}_d$ to be 0. And the velocity $\dot{y}$ must be travelling in a direction that approaches the sliding surface $s = 0$. We implement this control using the following function:

$$\epsilon = \begin{cases} \kappa s_{stop} & , (s\dot{e}) < 0 \text{ and} \\ & \quad |\dot{y}_d| < \dot{y}_{d\_min} \\ e_{min} & , \quad \text{otherwise} \end{cases} \tag{25}$$

where $\dot{y}_{d\_min}$ was measured from the experimental setup. For a stationary actuator the measured velocity varied by +/- 15 mm/s, therefore, $\dot{y}_{d\_min} = 20$ mm/s was selected. κ should theoretically be equal to 1, however experimentally it was found that the system required some additional damping. Therefore, its value was increased to $\kappa = 2$.

With this equation, if $\dot{y}_d \neq 0$, then the system is actively tracking y_d. However, if $\dot{y}_d \approx 0$, then it will reduce switching

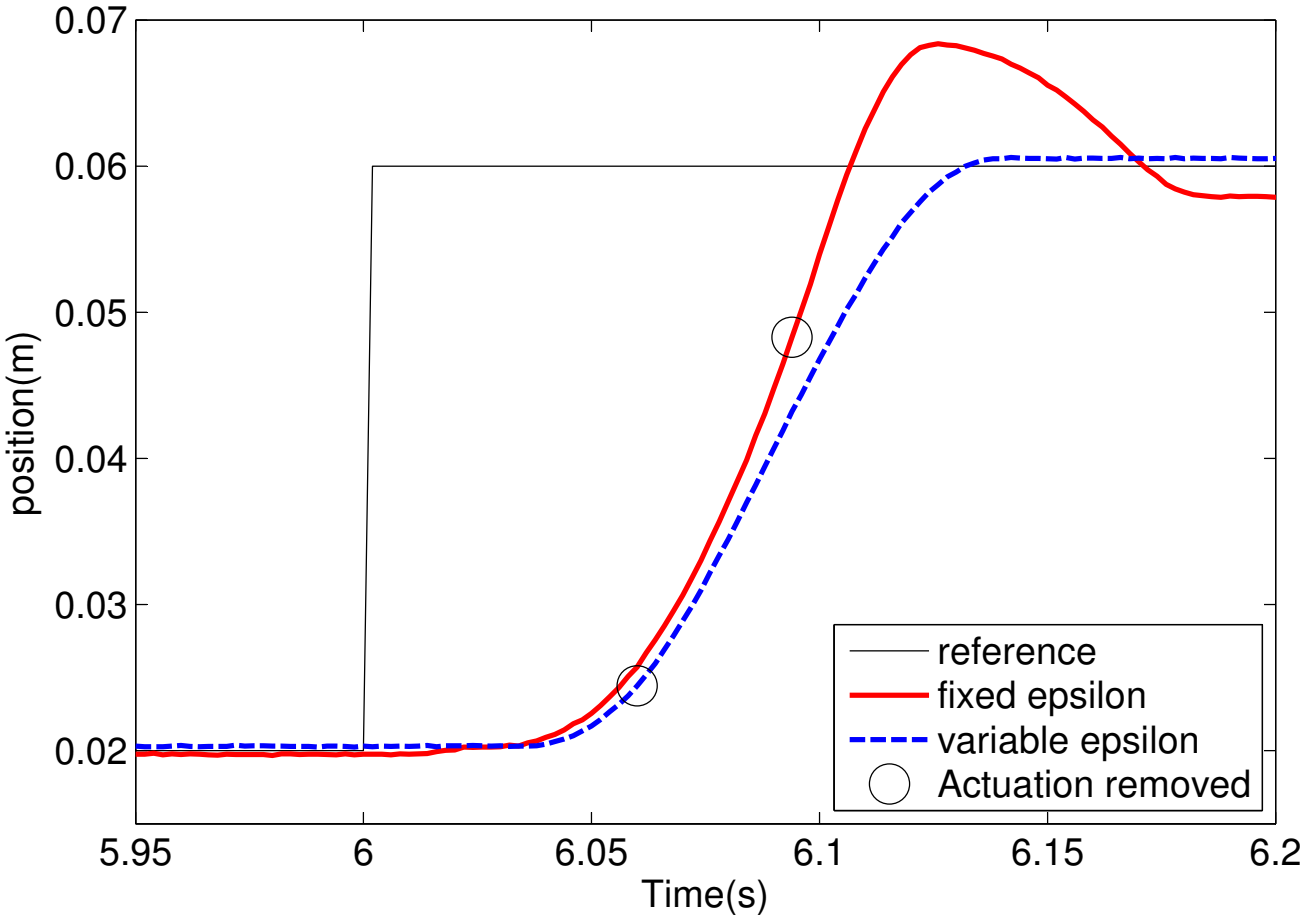

Fig. 5. Variable ϵ vs. fixed ϵ experimental results.

activity by stopping at the point that will settle on y_d without over-shooting the target. The equations (24) and (25) which calculate ϵ require that the values of P_N, P_P and y_d are measured.

Figure 5 shows the experimental results of testing the 7-mode controller with a fixed ϵ and a variable ϵ. The actuation is removed much sooner on the variable ϵ and as a result coasts to a stop on the desired position with no further correction required. However, with the 'fixed ϵ' controller actuation is removed too late and as a result it must immediately go in the reverse direction (mode 7) to try and reduce overshoot.

TABLE IV
TUNING PARAMETERS TABLE.

Par.	**Unit**	**Physical meaning**	**Effect on the performances**	**Tuning/Selection method**	**Experimental / Theoretical value**
τ	ms	Used when $\epsilon \geq \lvert s \rvert \geq \beta$, the minimum time between modes	Small τ increase switching and improves tracking performance	Calculated in simulation	40 ms / 40 ms
e_{min}	mm	The s threshold between actuation and no actuation	Large e_{min} reduces chattering and tracking precision	Desired tracking precision	1.0 mm / 1.0 mm
β	mm	The s threshold for using a higher drive potential	Small β strengthens piston actuation	(18) using an estimation of max($\dot{y}$)	3.0 mm / 3.7 mm

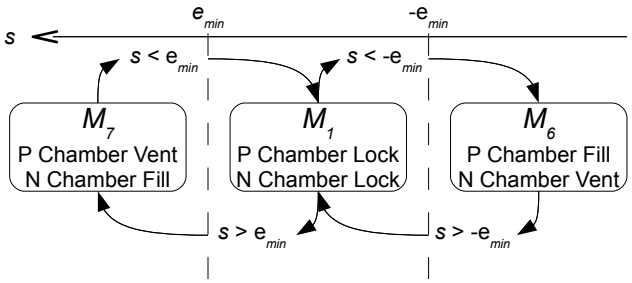

Fig. 6. 3-mode state diagram.

V. Simulation Study

To analyze the performance of the 7-mode controller described in this paper we will be comparing it against the original 3-mode controller it was based on. The state diagram for the 3-mode controller is show in Figure 6. The e_{min} shown in Figure 6 is from (25).

A. Simulation Parameters and Test Inputs

For our simulation, we selected the model parameters listed in Table V. These model parameters correspond to the experimental setup that will be used in Section VI.

TABLE V
System parameters table.

Var.	Value	Label
l	0.1 m	Chamber Length
T	23 C	Chamber Temperature
C_{val}	3.4×10^{-9} kg/(s Pa)	Mass Flow Rate Const.
P_S	$300,000$ Pa	Supply Air Pressure
P_E	$100,000$ Pa	Exhaust Air Pressure
k	1.2	polytropic constant
A	1.814 cm^2	Piston Cylinder Area
b_m	50 (N s)/m	Viscosity Coefficient
M_m	0.9 kg	Total Mass of load

For the controller $e_{min} = 1$ mm. To model our system we utilized the Simulink Simscape toolbox, which includes pneumatic elements.

There were a total of 3 different test inputs used:

1) Sine-wave:

$$y_d = 0.020 sin(2f\pi t) \tag{26}$$

2) Multi-sine wave:

$$y_d = \frac{0.030}{m} \sum_{i=1}^{m} sin(2\pi \frac{fi}{m} t) \quad m = 8 \tag{27}$$

3) Square-Wave:

$$y_d = \begin{cases} 0.020 & , |t| < T_{period}/2 \\ -0.020 & , T/2 \leq |t| < T_{period} \end{cases} \tag{28}$$

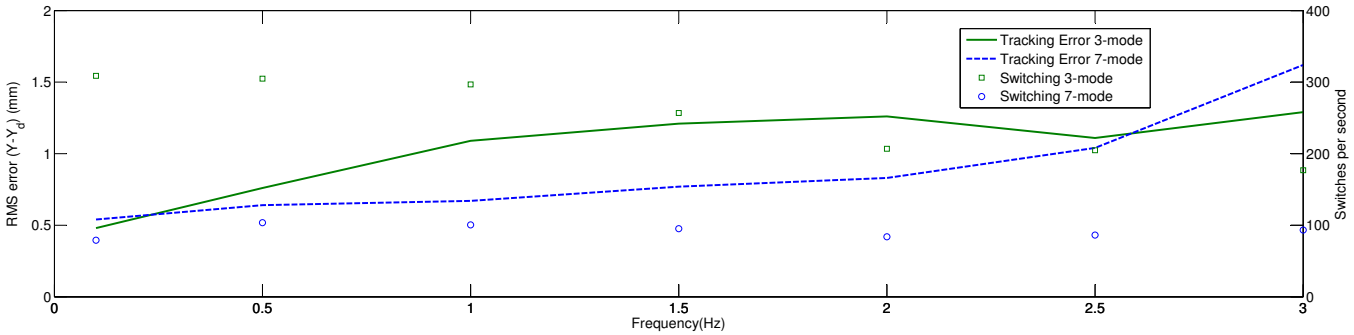

(a) Versus frequency.

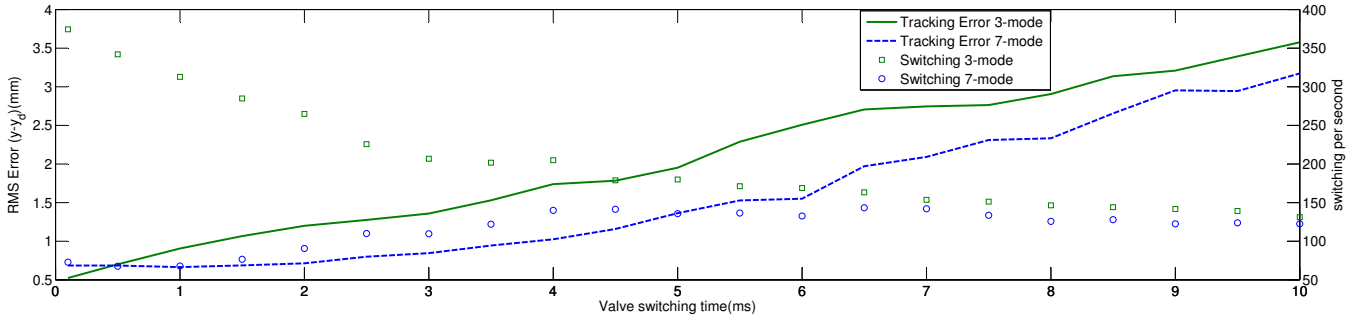

(b) For a 1.5 Hz sine-wave reference trajectory versus the valve response time.

Fig. 7. Position tracking and switching activity simulation results for a sine-wave reference trajectory.

Over a period of $T_{period} = 1/f$.

For our simulations, we selected $\omega = 100$ rad/s, $\xi = 0.5$, $\tau = 40$ ms, $\beta = 3.0$ mm, and $e_{min} = 1.0$ mm.

B. Simulation Results

The simulation was run utilizing the sine-wave test input with frequencies varying from 0.1 Hz - 3.0 Hz, the results of the simulations are charted in Figure 7(a). From these results, we find that for both the 3-mode and the 7-mode systems increasing the input frequency leads to an increase in RMS tracking. The inability of the systems to track y_d for higher frequency input sine-waves is due to a limitation of flow capability of the valves to drive the actuator at the higher velocities.

In the 7-mode system, for moderate differences between y_d and y, this difference may not be enough to switch from the $|s| > \beta$ region. As we can see this can cause a small tracking error in the 2-3 Hz range for the 7-mode system. This is one of the costs of using the 7-mode sliding control algorithm. The advantage of the 7-mode controller algorithm is the reduction in the solenoid valves switching as observed in Figure 7(a). At 1.5 Hz, this is equal to 63% reduction in switching activity and a 0.45 mm improvement in tracking error. The disadvantage of the 7-mode controller is that for small but rapid changes in the desired position y_d, the reduced drive of the actuator could cause a slightly bigger position error between the desired position and the actual position than the 3-mode controller.

To test the system with a more complicated signal, we used an input that is a summation of 8 sine-waves with 8 different frequencies.

For this simulation we will use $f = 1$ Hz. As we can see from Figure 8(a), both controllers have no trouble tracking the multi-sine wave; however, the switching activity (demonstrated by the open-close motions of the two valves in the P chamber)

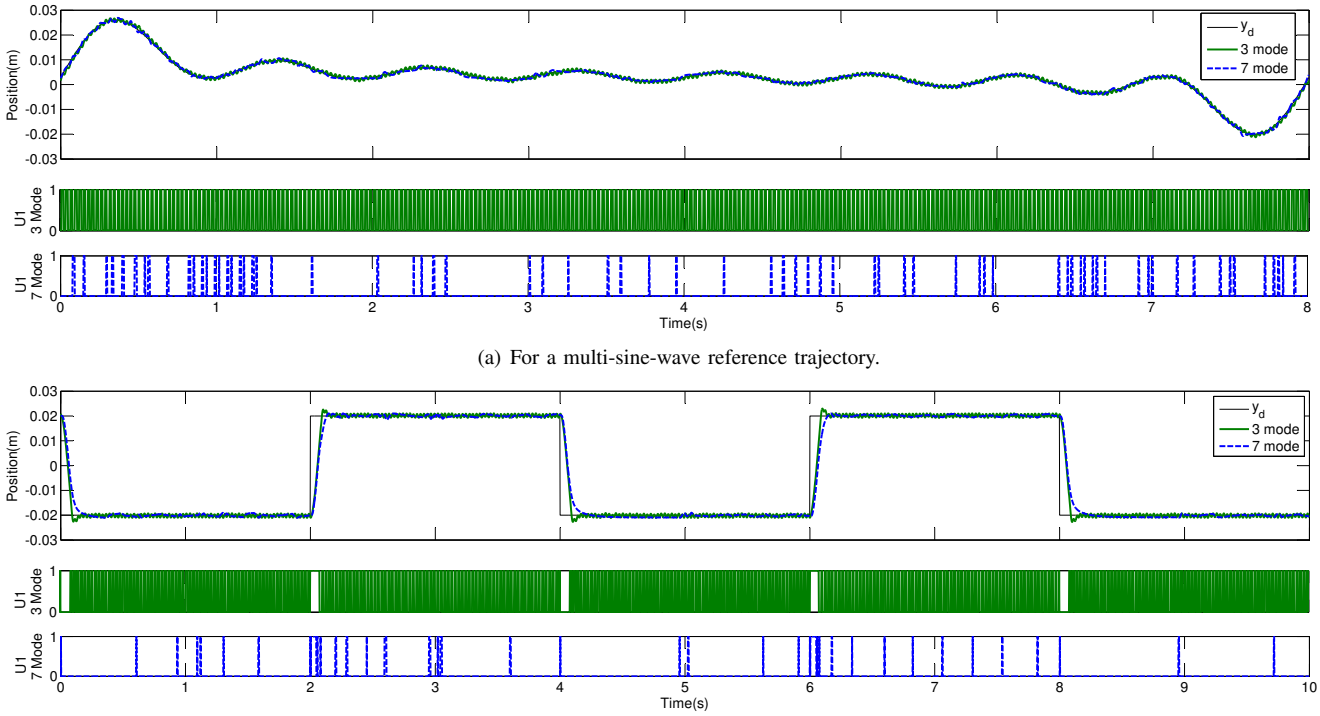

(a) For a multi-sine-wave reference trajectory.

(b) For a square-wave reference trajectory.

Fig. 8. Position tracking and switching activity Simulation results.

for the 7-mode controller is greatly reduced compared to the 3-mode controller. From the 3-mode controller to the 7-mode controller, there is a 75% reduction in solenoid switching activity.

To further test the controller, we utilized a square-wave function. The results of this testing can be observed in Figure 8(b). From the simulation, we find that the 3-mode controller has difficulty regulating at a fixed setpoint, which causes the switching to be on average 263.2 times per second. The 7-mode controller, however, minimizes the switches required to move between thresholds, resulting in a 76.6 switches per second on average. This switching per second count reflects the aggregated occurrence of switches in all 4 solenoid valves in each control modality.

The pneumatic system used in our experiments has solenoid valves that are switched at a rate of up to 500 Hz due to a valve switching time (response time) of 2 ms. In simulations, we have the flexibility to increase or decrease the valve switching time. To observe the effect of this, we have simulated a system with a 1.5 Hz sine-wave reference position and with the 3-mode and 7-mode controllers over a range of valve switching times varying from 0.1 ms to 10 ms. The results of these simulations have been plotted in Figure 7(b). It can be seen from these results that increasing the valve switching time increases the tracking error. It can also be seen from this plot that the switching activity for the 7-mode controller is always less than the 3-mode controller. The tracking error, in this figure, is found to be consistently better for the 7-mode controller versus the 3-mode controller.

VI. Experimental Testing

In this section, experiments with a 1-DOF system are reported. As illustrated in Figure 9, the setup consists of a pneumatic manipulator. The low friction cylinders (Airpel model M16D100D) have a 16 mm diameter and a 100 mm stroke. The piston

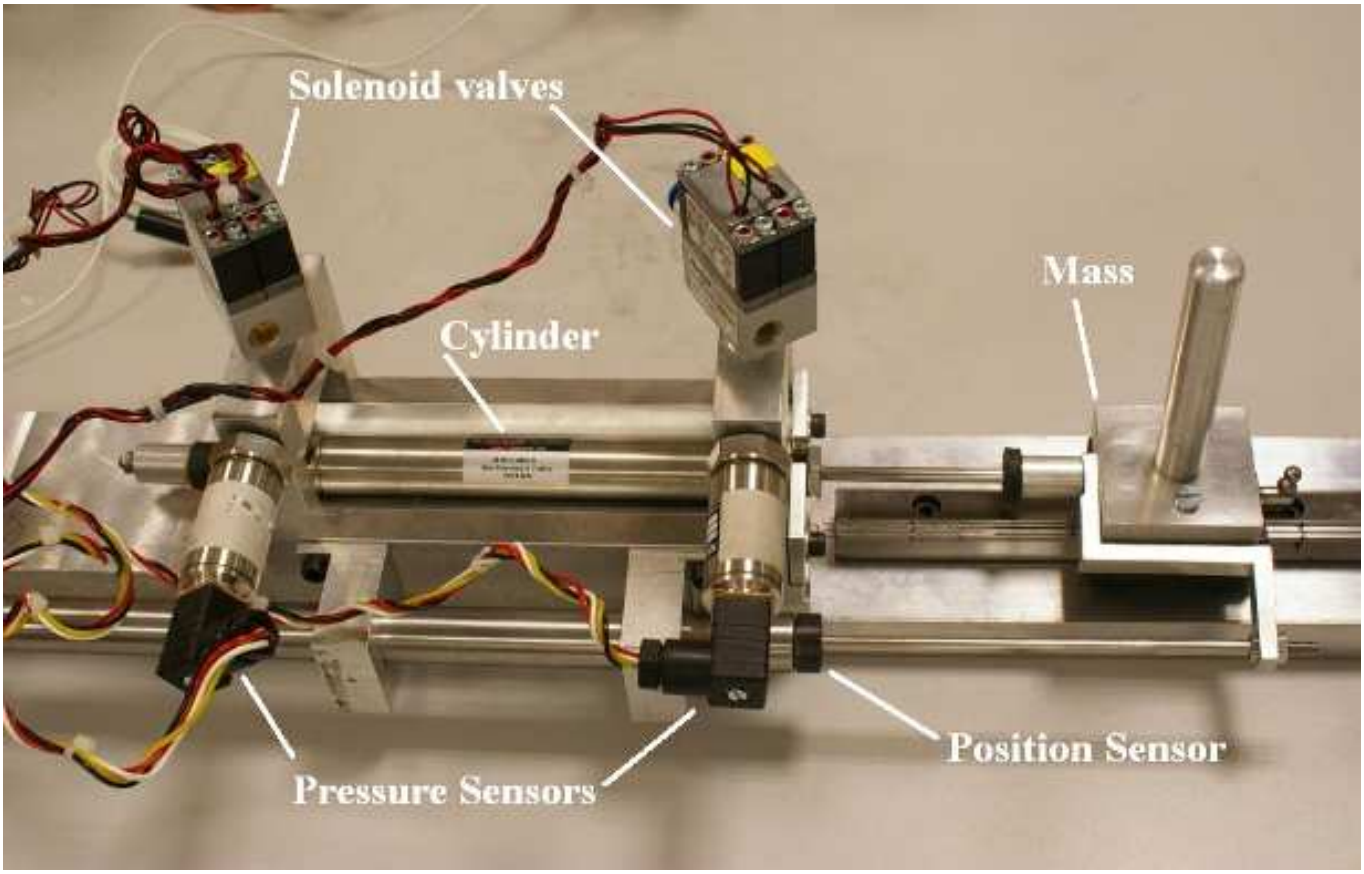

Fig. 9. Experimental setup.

is connected to a mass of approximately M = 900 g. The pneumatic solenoid valves (Matrix model GNK821213C3K) used to control the air flow have switching times of approximately 1.3 ms (opening time) and 0.2 ms (closing time). With such fast switching times, the on/off valves are appropriate for the purposes of the proposed control. In terms of sensors, a low-friction linear variable differential transformer (LVDT) is connected to the cylinder in order to measure the linear positions.

The controller is implemented using a dSPACE board (DS1104), running at a sampling rate of 500 Hz. This value has been chosen according to the open/close bandwidth of the switching valves and to guarantee an acceptable tracking response. For this experiment, the following controller parameters were selected: ω = 60 rad/s, ξ = 0.5, τ = 0.04 s, β = 3.0 mm, and e_{min} = 1.0 mm.

A. Experimental switching function

Our experimental setup has a position sensor. This setup does not have an accelerometer or velocity measurement. This section describes how the switching function s in (7) was obtained for experimental setups. The first derivative of the position error in (7) is computed through a backward difference method applied on the position signal followed by a de-noising second-order Butterworth filter with a cutoff frequency of 50 Hz. The second derivative is computed in the same way from the filtered first-derivative signal. The filter bandwidth was chosen to be large enough (50 Hz) with respect to the input's bandwidth of the system (less than 5 Hz) .

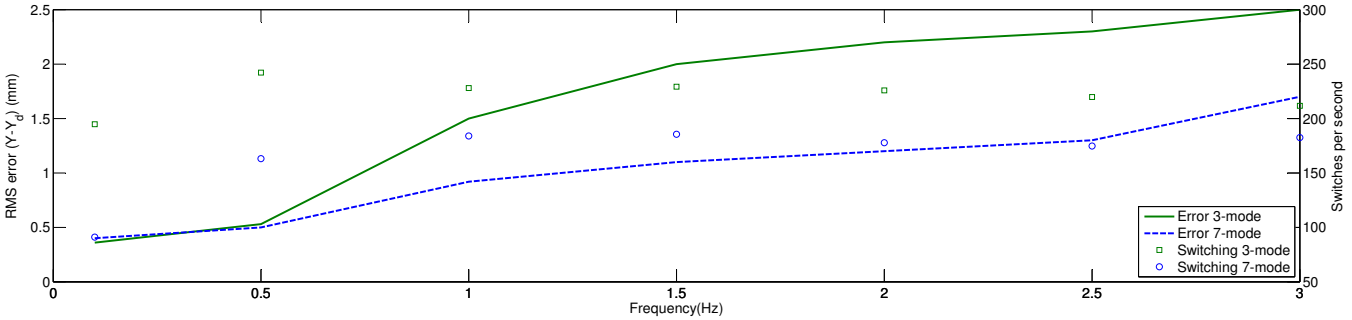

(a) No Load on Pulley

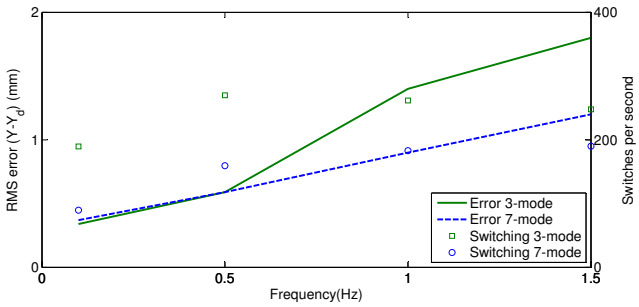

(b) 0.5 kg Load on Pulley

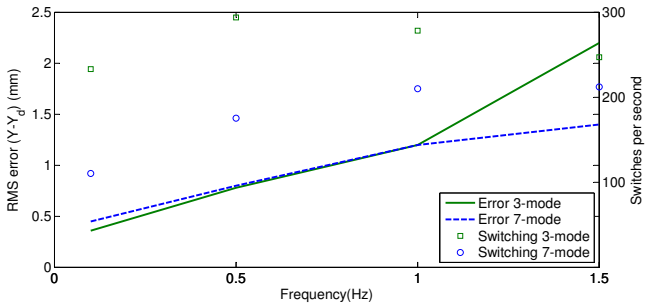

(c) 1.0 kg Load on Pulley

Fig. 10. Position tracking and switching activity experimental results for a sine-wave reference trajectory.

The following finite difference equations where then used to find the first and second derivatives.

$$\dot{e}_{filt}(j) = \frac{e_{filt}(j) - e_{filt}(j-1)}{T_{period}} \tag{29}$$

$$\ddot{e}_{filt}(j) = \frac{e_{filt}(j) - 2e_{filt}(j-1) + e_{filt}(j-2)}{T^2_{period}} \tag{30}$$

Where e_{filt} was the filtered tracking error. Substituting (29) and (30) into (7) produces

$$s_{exp} = \frac{\ddot{e}_{filt}}{\omega^2} + \frac{2\xi\dot{e}_{filt}}{\omega} + e_{filt} \tag{31}$$

B. Experimental Results

The experiment was run utilizing the sine-wave test input for the y_d desired position with frequencies varying from 0.1 Hz - 3.0 Hz. The recorded results from these experiments are charted in Figure 10(a). From these results, we find that for both the 3-mode and the 7-mode systems, increasing the input frequency increase the RMS tracking error (as shown in the simulated results). When we compare results for the 3-mode controller and the 7-mode controller, we can see that there was a notable improvement to tracking performance for the 7-mode controller; as well as a notable decrease in switching activity in the 7-mode case (as was demonstrated before in the simulated results).

The experiment was run utilizing a square-wave test input for the y_d desired position. The recorded results from these experiments are charted in Figure 11(b). From these results, we find that for the 3-mode case there is an 18% positive overshoot in the position tracking. For the 7-mode case the positive overshoot obtained was only 1.9%. This is the result of

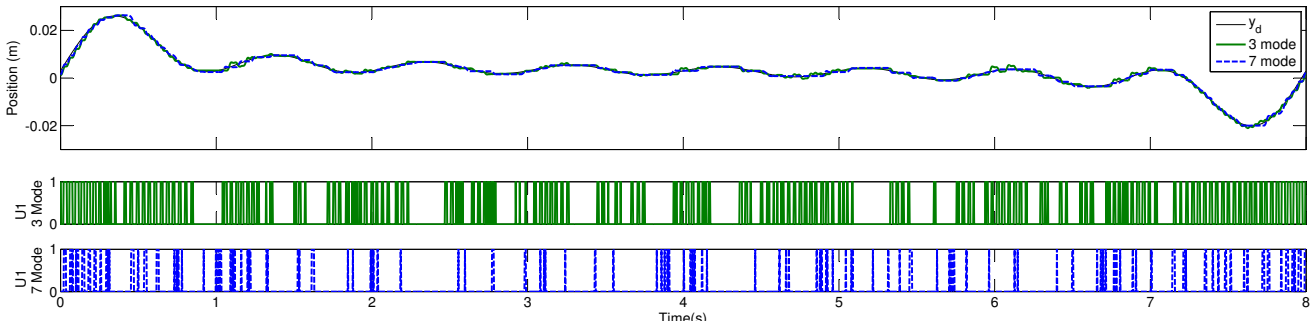

(a) For a multi-sine-wave reference trajectory

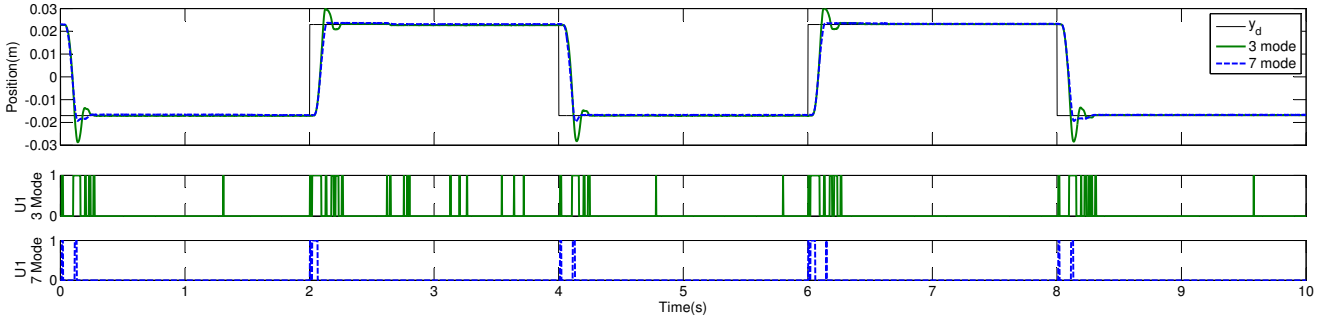

(b) For a square-wave reference trajectory

Fig. 11. Position tracking and switching activity experimental results.

the variable epsilon threshold applied to the 7-mode controller removing actuation sooner; allowing the actuator to coast to a stop onto the y_d position. This results in improved tracking performance and reduced switching activity.

To test the system with a more complicated signal, we used an input that is a summation of 8 sine-waves with 8 different frequencies. For this simulation we will use $f = 1$ Hz. As we can see from Figure 11(a), both controllers have no trouble tracking the multi-sine wave; however, the switching activity (demonstrated by the open-close motions of the two valves in the P chamber) for the 7-mode controller is reduced compared to the 3-mode controller as was seen in simulation. From the 3-mode controller to the 7-mode controller, there is a 48% reduction in solenoid switching activity.

To test the system's ability to reject external force disturbance, the experiment was run again utilizing the sine-wave test input with a weight attached to the actuator via a cord and pulley. The weights tested were 0.5 kg (see figure 10(b)) and 1.0 kg (see figure 10(c)). These weights applied a constant force that was approximately equal to gravity in the positive direction of the actuator. To prevent the weights attached to the actuator from swinging like a pendulum only frequencies from 0.1 Hz - 1.5 Hz were utilized. Tracking error was not significantly increased as a result of attaching the weights; valve switching activity was marginally increased.

The first objective of the simulation study was to validate the feasibility of the proposed control scheme before implementing it on the physical system. As in any other design, the simulation study helped to obtain an idea of the controller gains to be used in the experiments. Interestingly, while the simulated model was somewhat different from the experimental system, the good experimental results show the robustness of the proposed controller against unmodelled dynamics and model parameter uncertainties.

VII. Concluding Remarks

This paper proposed a sliding mode law for precise position control with minimal switching activity designed for use on a pneumatic actuator. The two-chamber actuator with four on/off solenoid valves had a total of sixteen possible modes only seven of which were considered functional and unique and were used for this particular control law. This controller uses four more additional modes compared to [17] that decrease the coarseness in the drive force for lower position tracking errors and reduce the open-close activity of the valves, increasing the valves' lifespan.

In order to evaluate this strategy, a comparison study has been performed relative to the 3-mode controller in [17] for a position tracking problem. The results show that the tracking accuracy in steady state is better in the case of 7-mode control than the 3-mode control. Also, the 7-mode controller was shown to lead to a significant reduction in the switching of the solenoid valves compared to the 3-mode control. This implied that the valve's lifetime will be longer and the overall reliability of the components will be better when the proposed control law is utilized.

The 7-mode based sliding control has been successfully implemented in simulations and then in experiments and good results have been achieved. Such a system would be an excellent choice for use as an actuator controlled inside an MRI-guided system.

For future work, we will control a dual-robot pneumatic teleoperation system using the proposed control law, and will investigate the effectiveness of the system in terms of high-fidelity transmission of critical haptic cues to the human operator in a delicate task such as needle insertion.

References

[1] M. Oura, Y. Kobayashi, J. Okamoto, M. Fujie, Development of MRI compatible versatile manipulator for minimally invasive surgery, in: Proceedings of 2006 First IEEE/RAS-EMBS International Conference on Biomedical Robotics and Biomechatronics, Tuscany, Italy, 2006, pp. 176–181.

[2] M. Uecker, S. Zhang, D. Voit, A. Karaus, K.-D. Merboldt, J. Frahm, Real-time MRI at a resolution of 20 ms, NMR in Biomedicine 23 (8) (2010) 986–994.

[3] M. Li, D. Mazilu, K. A. Horvath, Robotic system for transapical aortic valve replacement with MRI guidance, in: Proceedings of 2008 International Conference on Medical Image Computing and Computer-Assisted Intervention, New York, United States, 2008, pp. 476–484.

[4] B. T. Larson, A. G. Erdman, N. V. Tsekos, E. Yacoub, P. V. Tsekos, I. G. Koutlas, Design of an MRI-compatible robotic stereotactic device for minimally invasive interventions in the breast, Journal of Biomechanical Engineering 126 (4) (2004) 458–465.

[5] N. Yu, C. Hollnagel, A. Blickenstorfer, S. S. Kollias, R. Riener, Comparison of MRI-compatible mechatronic systems with hydrodynamic and pneumatic actuation, IEEE/ASME Transactions on Mechatronics 13 (3) (2008) 268–277.

[6] E. Hempel, H. Fischer, L. Gumb, T. Höhn, H. Krause, U. Voges, H. Breitwieser, B. Gutmann, J. Durke, M. bock, A. Melzer, An MRI-compatible surgical robot for precise radiological interventions, Computer Aided Surgery 8 (4) (2003) 180–191.

[7] J. A. Rosas-Flores, J. A. Flores-Campos, L. G. Corona-Ramírez, Optimal linearization of the dynamic behavior of an on/off actuated single pneumatic cylinder, in: Proceedings of 2008 5th International Conference on Electrical Engineering, Computing Science and Automatic Control (CCE 2008), Mexico City, 2008, pp. 380–385.

[8] A. Girin, F. Plestan, X. Brun, A. Glumineau, High-order sliding-mode controllers of an electropneumatic actuator: Application to an aeronautic benchmark, International Journal of Control 79 (2) (2006) 119–131.

[9] K. Xing, J. Huang, Y. Wang, J. Wu, Q. Xu, J. He, Tracking control of pneumatic artificial muscle actuators based on sliding mode and non-linear disturbance observer, IET Control Theory and Applications 4 (10) (2010) 2058–2070.

[10] H. K. Lee, G. S. Choi, G. H. Choi, A study on tracking position control of pneumatic actuators, Mechatronics 12 (6) (2002) 813–831.

[11] X. Shen, J. Zhang, E. J. Barth, M. Goldfarb, Nonlinear model-based control of pulse width modulated pneumatic servo systems, Journal of Dynamic Systems, Measurement, and Control 128 (2006) 663–669.

[12] M. Le, M. Pham, M. Tavakoli, R. Moreau, Sliding mode control of a pneumatic haptic teleoperation system with on/off solenoid valves, in: Proceedings of 2011 IEEE International Conference on Robotics and Automation (ICRA), Shanghai, China, 2011.

[13] A. Messina, N. I. Giannoccaro, A. Gentile, Experimenting and modelling the dynamics of pneumatic actuators controlled by the pulse width modulation (PWM) technique, Mechatronics 15 (7) (2005) 859–881.

[14] K. Ahn, S. Yokota, Intelligent switching control of pneumatic actuator using on/off solenoid valves, Mechatronics 15 (6) (2005) 683–702.

[15] M.-C. Shih, M.-A. Ma, Position control of a pneumatic cylinder using fuzzy PWM control method, Mechatronics 8 (3) (1998) 241–253.

[16] M. Taghizadeh, A. Ghaffari, F. Najafi, Improving dynamic performances of PWM-driven servo-pneumatic systems via a novel pneumatic circuit, ISA Transactions.

[17] T. Nguyen, J. Leavitt, F. Jabbari, J. E. Bobrow, Accurate sliding-mode control of pneumatic systems using low-cost solenoid valves, IEEE/ASME Transactions on Mechatronics 12 (2) (2007) 216–219.

[18] V. I. Utkin, Sliding mode control design principles and applications to electric drives, IEEE Transactions on Industrial Electronics 40 (1) (1993) 23–36.

[19] V. I. Utkin, H.-C. Chang, Sliding mode control on electro-mechanical systems, Mathematical Problems in Engineering 8 (4-5) (2002) 451–473.

[20] M. Le, M. Pham, R. Moreau, T. Redarce, Transparency of a pneumatic teleoperation system using on/off solenoid valves, in: Proceedings of 2010 19th IEEE International Symposium on Robot and Human Interactive Communication, Viareggio, Italy, 2010, pp. 15–20.

[21] P. Beater, Pneumatic Drives - System Design, Modelling and Control, Springer, Berlin, 2006.